AIAA

AIAA 2000-0419
Multidisciplinary High-Fidelity Analysis and
Optimization of Aerospace Vehicles,
Part 2: Preliminary Results

J. L. Walsh, R. P. Weston, J. A. Samareh, B. H. Mason,
L. L. Green, and R. T. Biedron
NASA Langley Research Center
Hampton, VA 23681

38th Aerospace Sciences Meeting & Exhibit
10-13 January 2000 / Reno, NV

MULTIDISCIPLINARY HIGH-FIDELITY ANALYSIS AND OPTIMIZATION OF AEROSPACE VEHICLES, PART 2: PRELIMINARY RESULTS

J. L. Walsh,[*] R. P. Weston,[†] J. A. Samareh,[‡] B. H. Mason,[§] L. L. Green,[¶] and R. T. Biedron[**]
NASA Langley Research Center, Hampton, VA 23681

Abstract

An objective of the High Performance Computing and Communication Program at the NASA Langley Research Center is to demonstrate multidisciplinary shape and sizing optimization of a complete aerospace vehicle configuration by using high-fidelity finite-element structural analysis and computational fluid dynamics aerodynamic analysis in a distributed, heterogeneous computing environment that includes high performance parallel computing. A software system has been designed and implemented to integrate a set of existing discipline analysis codes, some of them computationally intensive, into a distributed computational environment for the design of a high-speed civil transport configuration. The paper describes both the preliminary results from implementing and validating the multidisciplinary analysis and the results from an aerodynamic optimization. The discipline codes are integrated by using the Java programming language and a Common Object Request Broker Architecture compliant software product. A companion paper describes the formulation of the multidisciplinary analysis and optimization system.

Introduction

An objective of the High Performance Computing and Communications Program (HPCCP) at the NASA Langley Research Center (LaRC) has been to promote the use of advanced computing techniques to rapidly solve the problem of multidisciplinary optimization of aerospace vehicles. In 1992, the LaRC HPCCP Compu-

[*]Senior Research Engineer, Senior Member AIAA

[†]Senior Research Engineer

[‡]Research Scientist, Senior Member AIAA

[§]Aerospace Engineer, Member AIAA

[¶]Research Scientist, Member AIAA

[**]Research Scientist

tational AeroSciences (CAS) team began a multidisciplinary analysis and optimization software development project. Initially, the focus of the CAS project was on the software integration system, or framework, that was used to integrate fast analyses on a simplified design application. The sample application has been the High-Speed Civil Transport (HSCT, Fig. 1). Over the years, the CAS project has focused on progressively more complex engineering applications, with the application in the present study known as HSCT4.0. A companion paper[1] summarizes two previous applications, known as HSCT2.1[2] and HSCT3.5,[3] and presents the HSCT4.0 formulation. The HSCT has also been the focus of other research studies (see Refs. 4–10).

In 1997, the sample application[11] shifted to more realistic models and higher fidelity analysis codes. Preliminary results from implementing the HSCT4.0 application are presented in this paper. The HSCT4.0 application objective is to demonstrate simultaneous multidisciplinary shape and sizing optimization of a complete aerospace vehicle configuration by using high-fidelity finite-element structural analysis and computational fluid dynamics (CFD) aerodynamic analysis in a distributed, heterogeneous computing environment that includes high performance parallel computing. To this end, an integrated set of discipline analysis codes and interface codes has been formulated as a distributed computational environment for the design of an HSCT configuration. The analysis part of the design loop has been implemented into a software integration system that is known as CORBA Java Optimization (CJOpt)[12,13] and is based on a Common Object Request Broker Architecture (CORBA)[14] compliant software product and the Java™ programming language.

The formulation of the multidisciplinary design optimization problem and of its component analyses is presented in the companion paper.[1] The present paper is focused on the results obtained up to this point. First, an overview of the HSCT4.0 multidisciplinary optimization application is given and the validation test cases are described. Next, the overall analysis process is summarized, and results from the two validation cases are presented for many of the processes included in the complete analysis. There follows a discussion of

the present state of the sensitivity analysis and selected sensitivity analysis results. Finally, the optimization demonstration problem description and results—based on a nonlinear aerodynamic analysis—are presented.

<div align="center">

Overview
</div>

HSCT4.0 Model

The HSCT4.0 application considers a realistic aircraft concept and is a multidisciplinary application that integrates high-fidelity analyses representing aerodynamics, structures, and performance. For the HSCT4.0 application, a realistic model[*] that was a candidate for development as a commercial HSCT is used. This model was originally presented in Ref. 15. Other researchers are also investigating the use of multidisciplinary analyses, but with simple generic HSCT models.[4–10]

Figure 2 shows both the linear aerodynamics grid and the structural finite-element model (FEM) for half of the symmetric baseline HSCT4.0 model. A surface grid with approximately 1100 grid points for a linear code (USSAERO)[16] and a volume grid with approximately 600,000 grid points for a nonlinear code (CFL3D)[17] are used in combination for the aerodynamic analyses. For efficiency, only the wing and fuselage are modeled in the CFL3D calculation, but the corresponding linear aerodynamics model includes the tail surfaces; neither aerodynamic model includes the engines. An FEM with approximately 40,000 degrees of freedom (DOFs) is used with the structural analysis code (GENESIS®, a product of VMA Engineering[†]).[18] The engines are modeled as masses on beams. Eight laterally symmetric load conditions are used—one cruise load condition, six arising from maneuver conditions at +2.5g and −1g, and one representing a taxi condition. The Flight Optimization System (FLOPS)[19] code is used for modeling the aircraft performance.

Optimization Problem Description

The objective function of the HSCT4.0 optimization problem is to minimize the aircraft gross takeoff weight (GTOW) subject to geometry, structural, performance, and weight constraints. The geometry constraints

---

include constraints on fuel volume, ply-mixture ratio, airfoil interior thickness, takeoff ground scrape angle, and landing scrape angle. The structural constraints include buckling and stress constraints. The performance constraints include constraints on range, takeoff field length, landing field length, approach speed, a time-to-climb-to-cruise requirement, and noise. The weight constraints include constraints on various weight components. The total number of constraints is on the order of 32,000 with the majority being structural constraints. More detail on the constraints is included in the companion paper.

The HSCT4.0 application has 271 design variables for optimization—244 structural thickness variables and 27 shape variables. To limit the number of independent structural design variables, the optimization model is divided into 61 design variable zones, as shown in Fig. 3. Each zone consists of several finite elements. Thirty-nine zones are located on the fuselage and 22 zones are located on the wing (11 on the upper surface and 11 on the lower surface). Within each zone, four structural design variables are used. These structural design variables consist of three ply-thickness variables (a 0° fiber variable, a 90° fiber variable, and a variable that sizes the 45° and –45° fibers) and a core thickness variable. The ply orientations and composite laminate stacking sequence are shown in Fig. 4.

The 27 shape design variables (see Fig. 5) consist of two sets. The first set contains the nine planform variables shown in Fig. 5a—the root chord C_r, the outboard break chord C_2, the tip chord C_3, the semispan distance to the outboard break B_2, the leading edge sweep of the two outer wing panels SLE_2 and SLE_3, the total projected area of the three wing panels A_t, and the fuselage nose and tail lengths L_n and L_t. Note that the root chord also sets the length of the center fuselage section and that the wing semispan variable B_3 is dependent on other planform variables, including the total area.

The second set of shape design variables (see Fig. 5b) consists of control points that define the wing camber, thickness, twist, and shear at a set of airfoil shape definition points. The definition point locations for camber and thickness are identical, and those for shear and twist are identical. The 18 airfoil shape variables for HSCT4.0 are the vertical (z) perturbations of the camber, thickness, and shear from the wing baseline shape and the wing twist perturbation from the baseline shape in constant y planes. Note that the airfoil camber and thickness perturbations are smooth globally, while the twist and shear perturbations are linear between the line definition points.

<div align="center">

2

American Institute of Aeronautics and Astronautics
</div>

Optimization Formulation

***Optimization* Process** - Figure 6 illustrates the optimization procedure, which consists of a multi-disciplinary analysis (*Analysis*), gradient calculations (*Sensitivity Analysis*), and a gradient-based optimizer (*Gradient-Based Optimizer*). In the diagram, circles are used to indicate processes (or functions) and arrows show the data that are passed between processes. By convention, this paper uses italics for process names. Not all data passed between processes are explicitly shown—only enough data to indicate the required sequencing among processes. The outer loop in Fig. 6 represents one design "cycle," defined as analysis, evaluation of the objective function and constraints, sensitivity analysis, and optimization. The *Analysis* is summarized in a later section and described in detail in the companion paper.

***Sensitivity Analysis* Process** - The *Sensitivity Analysis* process provides the derivatives of the constraints and the objective function. This process is still being formulated.

***Gradient-Based Optimizer* Process** - The *Gradient-Based Optimizer* process,[20] based on a sequential linear programming (SLP) technique, consists of a general-purpose optimization program (CONMIN),[21] an approximate analysis that is used to reduce the number of full analyses during the optimization procedure, and some minor process steps. The approximate analysis is used to extrapolate the objective function and constraints with linear Taylor series expansions. This extrapolation is accomplished by using derivatives of the objective function and constraints (from the *Sensitivity Analysis* process) computed from the analysis at the beginning of each design cycle. Move limits are imposed on the design variables during the *Gradient-Based Optimizer* process to control any errors introduced by the linearity assumption.

Validation Test Cases

Two sets of initial design variables are used to validate that the disciplinary analysis processes described in the companion paper are integrated correctly. The term "integrated correctly" means that the values of the design variables and all quantities derived from the design variable values are passed from one process to another process correctly. The method of validation is to execute the *Analysis* process by using the CJOpt system and to compare the output from each process with the output from the original stand-alone code for that process and the same input for that process. The standalone discipline codes had been validated previously by comparisons with other engineering results. The integrated system validations include checks that the results obtained are reasonable, based on the experience of the discipline experts.

The first set of design variable values, known as the "Baseline" configuration, is based on the baseline FEM. It has zeros for all planform and airfoil shape variables, i.e. for all changes from the baseline shape. When this set of design variable values is used, the baseline shape and structural thicknesses are reproduced. The second set of design variable values, known as the "Higher Aspect Ratio" (HAR) configuration, results in a planform shape with a higher aspect ratio than the Baseline configuration and has structural design variable values that are increased based on the following arbitrary schema. If a design variable representing a 0° ply or a 45° ply is within 10% of its lower bound value, the value is increased by approximately 23%. If a design variable representing a 90° ply is within 10% of its lower bound value, the value is increased by approximately 145%. If a design variable representing the core is within 10% of its lower bound value, the value is increased by approximately 355%. The other design variables are unchanged. The HAR configuration is expected to have an increased weight as well as changes in stress and buckling responses.

Implementation Status

The analysis part of the HSCT4.0 multidisciplinary optimization process is fully operational within the CJOpt framework; it is executed on a heterogeneous set of computers linked by a local area network. All the component processes and the complete analysis have been validated as described above. The *Sensitivity Analysis* process for the complete system is still under development. It will link sensitivity derivatives from the component processes. The completion of the optimization application awaits the sensitivity analysis, although the *Optimization* process has been validated by using an aerodynamic analysis (described below) in place of the complete multidisciplinary analysis.

HSCT4.0 *Analysis* Process Validation

The HSCT4.0 *Analysis* process is formulated as the sequence of processes shown in the data flow diagram in Fig. 7 and summarized below. More details of the formulation are provided in the companion paper.

Analysis Process Summary

The *Analysis* process begins at the top of the data flow in the figure where the design variable values are prescribed. First, the *Geometry* process derives updated geometries and grids, from baseline geometries and grids, for use by later processes. Next, the *Weights* process uses the derived FEM and section properties to

calculate detailed weights and the center of gravity (c.g.) locations for specified flight conditions. The weights data are needed before the remaining processes can be executed. Next, the *Nonlinear Corrections* process can be executed. Note that the flow lines to this process are dashed; the dashed lines indicate that the *Nonlinear Corrections* process may not be executed in some design cycles due to the high computational time requirements. When this process is not run, the most recent nonlinear corrections continue to be used until an update is available.

Next the *Rigid Trim* process is executed for the cruise condition to determine the configuration angle of attack and the tail deflection angle that combine to yield a lift equal to the weight, with no net pitching moment. Once the *Rigid Trim* process has completed, the left branch in Fig. 7, comprising the *Polars*, *Performance*, and *Ground Scrape* processes, can proceed in parallel with the right branch, comprising the *Displacements*, *Loads Convergence*, and *Stress & Buckling* processes; the processes in each branch, however, must proceed sequentially.

The *Polars* process calculates the drag polars that are used by the *Performance* process. The *Performance* process uses the FLOPS code to calculate the mission performance metrics. The *Ground Scrape* process provides constraints so that the aircraft tail will not scrape the ground on takeoff or landing.

The *Displacements* process uses a finite-element analysis to generate linear static structural displacements due to applied aerodynamic and inertial loads for the cruise condition. These displacements are saved as a reference set for use in the *Loads Convergence* process. That process performs the aeroelastic trim calculations for the six noncruise load conditions, producing the aeroelastically converged loads on the aircraft. Lastly, in the *Stress & Buckling* process, stress and buckling constraints are computed for all elements contained in the 61 design zones on the fuselage and wing.

Table 1 shows typical execution times and computer types used for the *Analysis* process and the component processes within it. The *Nonlinear Corrections, Polars,* and *Loads Convergence* processes are the most time-consuming; the time for each of the other component processes is very small. If executed serially, the whole process would take almost 17 hours of wall clock time. By using coarse-grain parallelism within the *Loads Convergence* process, executing three load conditions (ten aeroelastic iterations each) simultaneously, the time for that process is reduced from 12 to 4 hours. The time for the *Polars*, *Performance*, and *Ground Scrape*

processes is effectively hidden by executing them in parallel with the *Displacements*, *Loads Convergence*, and *Stress & Buckling* processes. The *Nonlinear Corrections* process remains as the most time-consuming component process. For this reason, it is not executed in every design cycle. Without the *Nonlinear Corrections* process, the parallelized *Analysis* process executes in just 5 hours.

The following sections describe the validation of several component processes of the *Analysis* process. No results are presented for the *Rigid Trim*, *Displacements*, or *Ground Scrape* processes.

Geometry **Results**
The MASSOUD[22] shape parameterization methodology was developed for parameterizing changes from a baseline aircraft shape. Benefits of this approach are the ease of implementation for the parameterization of complex existing analysis models and grids, the relatively few shape design variables required, and the consistency of the resulting parameterization across all disciplines. The MASSOUD method has been successfully demonstrated for aerodynamic shape optimization, including analytical sensitivity derivative computations, with a structured CFD grid[23] and with an unstructured CFD grid.[24]

Figure 8 shows the FEM for the Baseline configuration on the left-hand side and the HAR configuration, as modified by using the MASSOUD method, on the right-hand side. The heavy solid lines represent the baseline locations of the hexahedral solid elements that control the planform variation. Note that the large number of elements in the FEM are smoothly perturbed by changes in the 27 shape design variables.

Weights **Results**
The as-built weight of a component includes the as-built structural weight, plus nonstructural, systems, payload, and fuel weights, of which only the structural and fuel weights change with the design variables in the current formulation. The as-built structural weight of a component includes both the theoretical FEM structural weight and structural weight increments for production splices, local pad-ups, side-of-body joints, adhesives, paints, materials for damage tolerance, sealants, and fasteners essential in building the aircraft. Non-structural weight items include windows, landing gear doors, access doors, seat tracks, fuel tank baffles, and passenger doors, and system attachment fittings.[25] The theoretical FEM structural weights are calculated by the GENESIS® code as applied nodal forces due to a gravity load vector. The remaining weights are calculated by empirical weight estimation methods.

In order to obtain the as-built weights, the FEM is divided into the 14 weight calculation regions shown in Fig. 9. The as-built weight distributions for HSCT4.0 are defined by a set of 42 files, each of which corresponds to one of the 14 regions. Some regions have more than one associated file. For example, the four files associated with region 1 (part of the inboard wing) represent the structural weight distribution, the nonstructural weight distribution, the systems and equipment weight distribution, and the wing main landing gear weight distribution.

Only the theoretical FEM structural weights of regions 1 through 5 are changed directly by the design variables. The theoretical FEM structural weights of regions 8 through 11 change as these regions stretch and/or contract to remain consistent with geometric changes in regions 1 and 2. Under the current formulation, the structural weight does not change in regions 6, 7, 12, and 13, and none of the nonstructural, systems, or payload weights change. The inboard wing fuel weight changes in proportion to the available fuel volume as the geometry changes. Also, the fuel weight files are the only ones that differ between the two mass cases (cruise and GTOW) considered in HSCT4.0. These two mass cases are obtained by adding the payload weight and the appropriate files of fuel weight to the operational empty weight (OEW).

Figure 10 shows the percent change of the HAR configuration relative to the Baseline configuration for several as-built weight items. For comparison, the figure also shows percent changes in three geometric items that are generally significant in empirical weight estimation methods: the wing average thickness-to-chord ratio, taper ratio, and aspect ratio. Note that the outboard wing as-built structural weight, which has the largest relative weight increase (about 19%), is well correlated with the wing aspect ratio increase; all other weights change by 5% or less.

It is important to realize that a change in the aircraft structural weight has a relatively small effect on the aircraft GTOW, which is to be minimized in the optimization. The entire as-built structural weight is only about 12% of GTOW and 27% of the OEW, which excludes the payload and fuel weights. Almost half of the structural weight is the as-built structural weight increment, so it is important that this increment is included in the optimization. The payload, systems, and non-structural weight increments are held constant in the current formulation. The fuel is the most significant contributor to weight because it is about 30% of the cruise weight and about 46% of the GTOW. This effect can be seen in Fig. 10, where the cruise weight is almost unchanged and the GTOW actually

decreases along with the fuel weight, although the structural weights increase.

Nonlinear Corrections **Results**

For efficiency, a *Nonlinear Corrections* process is used that requires at most one computationally intensive, nonlinear CFD calculation per load condition during each design cycle. The result is used to calculate a nonlinear correction relative to the corresponding linear aerodynamics calculation. The *Nonlinear Corrections* process uses the CFL3D code in the Euler (inviscid) mode to capture nonlinear aerodynamics. The computed pressure distribution for each load condition is transferred to the panels of the linear aerodynamics grid while maintaining the same total normal force and pitching moment. The nonlinear correction is the panelwise difference between the nonlinear aerodynamics pressure distribution and the corresponding linear aerodynamics pressure distribution from the USSAERO code. This correction is applied many times during the iterations of the *Loads Convergence* process.

Figure 11 shows the upper surface distribution of the nonlinear corrections, expressed as a correction pressure coefficient, for the Baseline and HAR configuration cruise conditions and the load factor extremes of 2.5g and –1g. Because the primary aerodynamic changes are accounted for by the linear aerodynamic calculations, the differences between the correction distributions are modest between the two configurations, despite significant wing shape changes.

For the first *Analysis* process cycle, the nonlinear aerodynamics corrections are set to zero. Therefore, all the following results use zero nonlinear corrections.

Polars **Results**

In the *Polars* process, the cruise lift and drag from the *Rigid Trim* process are augmented by calculating a table of drag polars for a range of Mach numbers and of lift coefficients; this table provides input to the calculations in the *Performance* process. The lift-dependent drag at each specified Mach number is determined by interpolating between USSAERO calculations for a set of angles of attack and tail deflection angles to determine the trimmed drag coefficients at the specified lift coefficients. This lift-induced drag contribution is then combined with the lift-independent drag contributions of skin friction drag, wave drag,[26] and other miscellaneous drag increments to obtain the drag polars. Nonlinear corrections are not calculated for the polars because of the computational time that would be required. The 1g cruise shape is used for all of the *Polars* process calculations.

Figure 12 shows the polar curves for the Baseline and the HAR configurations. These curves require 320 USSAERO executions in addition to the lift-independent calculations of skin friction, wave, and miscellaneous drags. The 1–2% decreases in drag values for the HAR configuration are primarily a result of lower induced drag due to the higher wing aspect ratio.

Performance Results

The *Performance* process uses the FLOPS code with the input geometry, weight, and drag polar data for the current geometric configuration to calculate a variety of mission performance metrics. These metrics include the range, the takeoff and landing field lengths, the aircraft noise, the excess thrust, and the takeoff and landing speeds (used by the *Ground Scrape* process).

Figure 13 shows the percent change of the HAR configuration relative to the Baseline configuration for several of the performance metrics. The excess thrust shown is needed so that the aircraft has more available thrust than drag at all times during the climb to cruise. In this example, only the approach and climb-out excess thrust, second-segment excess thrust, and thrust-to-weight ratios increase with the change from the Baseline configuration to the HAR configuration. The maximum change occurs for the second-segment excess thrust, which increases by about 3.5%; all other changes are about 1.5% or less. The decrease in range is well correlated with the decrease in fuel volume, as expected; the decrease in landing field length is well correlated with the decreases in the approach speed and the GTOW (from Fig. 10). The changes in the wing loading and thrust-to-weight ratio are as expected, given the decrease in GTOW (Fig. 10), while the wing reference area and thrust are held constant.

Loads Convergence Results

In the *Loads Convergence* process, the trimmed aerodynamic loads for the six noncruise load conditions, excluding the taxi condition, are determined from an iterative aeroelastic analysis. An aeroelastic analysis is required because the structural displacements depend on the aerodynamic pressure loading and the aerodynamic pressures depend on the displaced shape of the aircraft. Because of this mutual dependency between aerodynamic pressures and structural displacements, an iterative process is used to determine the converged aerodynamic loads at each load condition. Results are presented for the two of the six load conditions that represent the load factor extremes of 2.5g and –1g. Of the six load conditions, these two load conditions are the slowest to converge.

Figure 14 shows the convergence history through ten aeroelastic iterations in terms of the scaled angle of attack and the scaled tail deflection angle for the Baseline and the HAR configurations. As shown in Figs. 14a and 14c, both the angle of attack and the tail deflection angle of the Baseline configuration at the 2.5g load condition have essentially converged after five aeroelastic iterations. For the –1g load condition, more iterations are required. However, for the HAR configuration, more than 10 aeroelastic iterations will be required in the current formulation. The number of iterations required can be reduced by applying a relaxation factor.

Figure 15 shows aeroelastically displaced wing shapes for both the Baseline and the HAR configurations under the same two load conditions. These results correspond to iteration 10 of Fig. 14. The left half of each part of the figure shows the displaced FEM grid that results from application of the aerodynamic loads: the right half shows the corresponding displaced linear aerodynamics surface grid that is used to compute the aerodynamic loads. This figure demonstrates that the structural and aerodynamic shapes of the wing are consistent. This consistency indicates that the aeroelastic iteration is converged. (The fuselage shapes are not consistent because the fuselage aerodynamic surface is not displaced in the current formulation, while the FEM fuselage is displaced; the fuselage shapes will be made consistent in the next phase of the project.)

Stress & Buckling Results

In the *Stress & Buckling* process, a fuselage cabin pressure is added to each of the six converged load conditions from the *Loads Convergence* process, and the total is multiplied by a 1.5 factor of safety to produce a set of augmented loads. The GENESIS® code uses this set of augmented loads and a taxi load to compute stress failure indices and stress resultants for each element in the 61 design zones.

Stress and buckling results for both the Baseline and the HAR configurations are presented in Figs. 16–19 for the 2.5g and –1g load conditions. Elements shown in white in the plots are not sized. Stress result plots represent the Hoffman stress failure index (SFI)[18] values. The GENESIS® code computes one SFI value for each ply in a sized element (a total of eight values per element) for each load condition. Only the maximum layerwise SFI value in each element is retained. Buckling result plots represent a normalized buckling load factor (BLF), which is defined in the companion paper. One BLF value is computed per sized finite element per load condition. Retaining one SFI and one BLF value for each element for each of

seven load conditions would result in 31,640 structural constraints. For simplicity in this paper, stress and buckling results are presented as the largest SFI and the largest BLF per design zone for each load condition. In Figs. 16 to 19, SFI and BLF values above the critical level (1.0) indicate that the constraint has been violated.

In Fig. 16a, only one design zone on the upper wing surface of the Baseline configuration has a stress constraint violation for the 2.5g load condition. As shown in Figs. 16b and 17b, no stress constraint violations occurred in the Baseline or the HAR configurations for the –1g load condition. Three zones on the wing upper surface and one on the lower surface at the inboard-outboard break had moderate stress violations for the HAR configuration for the 2.5g load condition, according to Fig. 17a.

According to Fig. 18a, two design zones on the side and one on the lower surface of the fuselage have moderate buckling constraint violations, and one zone on the lower surface of the fuselage has a severe buckling constraint violation for the Baseline configuration for the 2.5g load condition. In Fig. 18b, three buckling constraint violations occur in the Baseline configuration on the fuselage for the –1g load condition. No buckling constraints are violated for the HAR configuration for either load condition, as shown in Fig. 19.

This section has summarized the status of the *Analysis* process validation. The next section discusses the status of the *Sensitivity Analysis* process.

Sensitivity Analysis Results

Sensitivity Analysis **Process**
The *Sensitivity Analysis* process that provides the derivatives of the constraints and the objective function is currently under development. Because not every analysis is a direct function of the design variables, it is necessary to obtain the constraint and/or objective function derivatives by chain-ruling the component derivatives. The plan is to use analytical derivatives whenever possible, either by hand differentiating the equations or by using the automatic differentiation tools ADIFOR[27–29] and ADIC,[30] to obtain the component derivatives from any analysis for which source code is available. For example, the geometry tools MASSOUD and CSCMDO[31] have been differentiated with the ADIC tool. Similarly, representative versions of the FLOPS code (used in *Weights* and *Performance* processes), the USSAERO code (used for linear aerodynamics calculations), and the CFL3D code (used for nonlinear aerodynamics calculations) have been

differentiated with the ADIFOR tool. These derivatives have been verified for accuracy by comparisons with finite-difference approximations. Thus, sensitivity derivatives for the majority of the codes used in the *Sensitivity Analysis* process are expected to be readily available.

The GENESIS® source code is not available for ADIFOR processing, leading to the major difficulty in obtaining derivatives for the HSCT4.0 application: choosing a method to obtain the total stress and buckling constraint derivatives. The total stress and buckling constraint derivatives depend on component derivatives obtained by differentiating the equilibrium equation for linear static analysis with respect to the design variable vector $\mathbf{V}$:

$$\frac{\partial \mathbf{K}}{\partial \mathbf{V}} \mathbf{u} + \mathbf{K} \frac{\partial \mathbf{u}}{\partial \mathbf{V}} = \frac{\partial \mathbf{f}}{\partial \mathbf{V}} \tag{1}$$

where $\mathbf{K}$ is the stiffness matrix, $\mathbf{u}$ is the vector of nodal displacements, and $\mathbf{f}$ is the applied load vector. Normally, in structural optimization, it is assumed that constant loads are used, so $\partial \mathbf{f}/\partial \mathbf{V} = 0$, and methods exist in the GENESIS® code for obtaining the stress and buckling constraint derivatives based on that assumption. The plan for the HSCT4.0 project is not to assume constant loads, because the trimmed aeroelastic loads from the *Loads Convergence* process are expected to vary with the shape design variables. One method is to obtain $\partial \mathbf{f}/\partial \mathbf{V}$ for the stress and buckling constraint derivatives by finite differences; this method can be computationally intensive for 271 design variables. An alternate, approximate method to incorporate non-zero $\partial \mathbf{f}/\partial \mathbf{V}$ is to exploit the modal approach described in Ref. 9.

Sample sensitivity results from codes that may be used in the *Sensitivity Analysis* process are presented next. The analytical sensitivity derivatives have been verified by comparisons with finite-difference results.

Geometry Sensitivities
The *Geometry* process calculates shape, structural, and miscellaneous geometries. For the shape geometry, exact sensitivity derivatives required by a gradient-based optimizer are defined as the partial derivatives of the geometry model or grid-point coordinates with respect to a design variable. The ADIC tool was applied to MASSOUD to augment it with these analytic sensitivity derivatives. Figure 20 shows the sensitivity derivative, $\partial x/\partial C_r$, of the x coordinate of the FEM nodes with respect to root chord. Because the aft fuselage is fixed, $\partial x/\partial C_r$ is small near the inboard trailing edge. The maximum $\partial x/\partial C_r$ is near the wing

tip. Because in the HSCT4.0 formulation[1] the total area is a design variable, the root chord change has a direct impact on the span of the outboard wing panel. Figure 21 shows the volume grid and $\partial x/\partial C_r$ for the CFD grid. The behavior for $\partial x/\partial C_r$ is the same as for the FEM.

The structural geometry sensitivities (ply mixture and airfoil interior thickness sensitivities) are computed analytically. It is expected that the remaining geometry codes can also be augmented to produce analytical derivatives.

Weights Sensitivities

The FLOPS code used as part of the *Weights* process has been differentiated with the ADIFOR tool. The resulting code can compute a variety of exact derivatives of empirical weights metrics with respect to a variety of independent parameters including planform and wing section geometry inputs and weight inputs.

Table 2 shows a sample of normalized weights sensitivity derivatives computed by the ADIFOR-generated FLOPS code. The derivatives are normalized as $(x/y)*(\partial y/\partial x)$, where x is the value of independent parameter, and y is the value of the dependent variable. The independent input parameters are the fuselage length (XL), the width of the fuselage (WF), the depth of the fuselage (DF), the GTOW, the aspect ratio (AR), the reference wing area (SW), and the inboard wing leading edge sweep angle (SWEEP). The dependent variables are the wing weight (WING), the fuselage weight (FUSELAGE), the total structural weight (STRUTOT), the total systems weight (SYSTOT), and OEW.

As shown in the table, the normalized derivatives are generally of the same order of magnitude, with both positive and negative derivatives represented. The actual computed derivatives span several orders of magnitude. Computation of a derivative matrix for 115 independent by 33 dependent variables requires about 4 minutes on a Silicon Graphics R10000™ workstation. For comparison, an analysis-only execution of the FLOPS code requires about one minute on the same workstation. Thus in this case, the use of ADIFOR provides a thousand-fold speedup over the use of finite differences.

The GENESIS® code, the other major part of the *Weights* process, does not have the capability to generate the theoretical FEM nodal weight sensitivities. A method for calculating the theoretical FEM nodal weight sensitivities is being formulated.

Nonlinear Analysis Sensitivities

The CFL3D code has been differentiated by using the ADIFOR tool. The resulting derivatives have been validated by using finite differences.[23] This differentiated code is utilized in a following section for an aerodynamic optimization of the HSCT4.0 configuration.

Performance Sensitivities

The differentiated FLOPS code that is used for weights sensitivity is also used to calculate a variety of exact derivatives of performance metrics. Table 3 shows a sample of sensitivity derivatives of normalized performance metrics. The performance derivatives in this table are normalized by the same method as the weights derivatives in Table 2. The independent parameters (GTOW, AR, and SW) are defined in the preceding Weights Sensitivities section. The dependent variables in Table 3 are a combined noise figure of merit (COMBND), the aircraft range (RANGE), the approach speed (VAPP), the takeoff field length (FAROFF), the landing field length (FARLND), the approach/climb-out excess thrust (AMFOR), and the second-segment excess thrust (SSFOR).

As can be observed in Table 3, the normalized derivatives in the sample are generally within a few orders of magnitude, with both positive and negative derivatives represented. Though spanning fewer orders of magnitude than the computed weights derivatives above, the actual computed performance derivatives again span several orders of magnitude.

Stress & Buckling Sensitivities

The codes used to perform structural sensitivity analyses and post-process the results are currently being tested by comparisons with sensitivities computed by finite differences. Although the GENESIS® code can been used to generate stress and stress-resultant sensitivities for $\partial \mathbf{f}/\partial \mathbf{V} = 0$ (i.e., constant load vector; see Eq. 1), the current HSCT4.0 plan is not to use a constant load vector. Only the sensitivities of the laminate with the largest SFI value for each element are post-processed by the stress sensitivity code. The BLF formulas in the companion paper are differentiated by the chain rule with respect to the shape and structural design variables to form the buckling sensitivities. The resulting BLF sensitivity equations include terms for stress resultant sensitivities; the BLF sensitivity code uses the stress-resultant sensitivities generated by the GENESIS® code for these terms. But again, these are based on a constant load vector. The constant load vector assumption will be tested, and if necessary, an alternative sensitivity method, such as that described in Ref. 9, will be developed.

American Institute of Aeronautics and Astronautics

Aerodynamic Shape Optimization Results

One aspect of any optimization formulation is the proper choice for the upper and lower bounds on the design variable values. For the HSCT4.0 application structural design variables, these upper and lower bounds are easy to determine. However, the appropriate upper and lower bounds for the shape design variable values are not so readily determined. Therefore, as a way to help in specifying upper and lower values for the shape design variables, as well as to test the *Optimization* process (Fig. 6) with a CFD analysis, an aerodynamic shape optimization problem was formulated.

Aerodynamic Shape Optimization Formulation

This optimization problem uses the HSCT4.0 set of 27 shape design variables in the same *Optimization* process as the complete HSCT4.0 application (Fig. 6), but with a small subset of the *Analysis* processes shown in Fig. 7. No structures or performance calculations are used.

The objective is to minimize the pressure drag on the Baseline configuration (again, wing-body only) at the cruise Mach number of 2.4. The lift is held fixed at the baseline cruise level. This information, along with the *Analysis* and *Sensitivity Analysis* results, is fed to the optimizer, which determines a new set of design variables that is used to start the process again. The process is repeated until no significant drag reduction is observed in subsequent optimization cycles. Other than upper and lower bounds on the design variables, no constraints are applied.

Analysis **Process** - Fig. 22 shows the nonlinear aerodynamic-only *Analysis* process that replaces the multidisciplinary *Analysis* process of Fig. 7. The *Geometry* process here consists only of the MASSOUD shape parameterization code combined with the CSCMDO[31] volume-grid deformation code. The *Nonlinear CFD Analysis* process uses the CFL3D code.

The inviscid aerodynamic calculations are done on a 129 X 177 X 25 grid split into 32-equal sized blocks and run on 32 processors of a Silicon Graphics Origin 2000™. In this case, lift coefficient was held fixed by using an option in the CFL3D code that adjusts the angle of attack to generate a specified lift coefficient. The drag computed within CFL3D was passed on to the optimizer.

Sensitivity Analysis **Process** - Figure 23 shows the aerodynamic shape optimization *Sensitivity Analysis* process, which uses analytic sensitivity derivatives generated by the ADIC tool for the *Geometry* process

and by the ADIFOR tool for the *Nonlinear CFD Sensitivity Analysis* process. The drag coefficient gradient with respect to each of the 27 design variables was computed within the CFL3D code and passed on to the optimizer.

Gradient-Based Optimizer **Process** - The *Gradient-Based Optimizer* process is based on the same sequential linear programming process described above for the complete HSCT4.0 application.

Aerodynamic Optimization Results

The specific version of the nonlinear aerodynamic code used in HSCT4.0 is CFL3Dv4.1hp. This version of the code has been ported to parallel computer architectures, where it has been demonstrated to scale well with the number of processors in both the function and derivative modes.[23] Figure 24 illustrates the speedup obtained by using multiple processors for gradient calculations with respect to the 27 shape design variables considered in HSCT4.0. For an increasing number of processors, at least up to the maximum of 32 used for the scaling study, a nearly linear speedup is observed. With 32 processors, the function calculation shows a superlinear speedup. This superlinear speedup is not unusual for large problems—as the per-processor memory requirements decrease, the problem fits more completely into cache, so that the per-processor floating point operation rate improves over that for fewer processors. However, based on past experience, it is expected that for a sufficiently large number of processors the speedup will degrade to sublinear as communication time becomes a larger part of the overall execution time. The speedup obtained by using multiple processors is crucial to successful use of high-fidelity CFD methods in the optimization process.

Figure 25 shows the design cycle history for aircraft drag, as measured relative to the baseline values. It can be seen that the drag has been reduced by approximately 7.5% relative to the baseline. With CFL3D executing in parallel on 32 processors, each design cycle required approximately 1 hour of CPU time, the bulk of which was the CFL3D computation of the 27 gradients. Although the optimizer has not fully converged for this case, the convergence history from 20 design cycles suggests that little additional reduction in drag would be obtained from additional design cycles.

Figure 26 shows a comparison of the baseline and final surface pressures on both the upper and lower surfaces. The planform changes that occurred between the initial and final design cycles are also evident. The primary effect on the planform has been to increase the

American Institute of Aeronautics and Astronautics

span and aspect ratio slightly and to move the outer wing leading edge break to a more inboard spanwise location. Although not evident in the figure, the wing thickness has been slightly reduced.

Concluding Remarks

The HSCT4.0 project at NASA LaRC has demonstrated the multidisciplinary analysis of a complex aerospace configuration with high-fidelity analysis methods. This multidisciplinary analysis has been executed in an automated system on a network of heterogeneous computers. The HSCT4.0 project team has validated the complete analysis by a rigorous, step-by-step validation of each process within the overall system against its previously validated stand-alone counterpart; this validation has included checking that all files passed between individual components are correctly identified and managed. This validation process was crucial to ensuring that the entire system functioned as desired. Additional checks showed that the results obtained were reasonable, based on the experience of the discipline experts. The HSCT4.0 project has demonstrated that analytic sensitivity derivatives can be obtained for many of the component parts by applying the ADIFOR and ADIC tools to those components and that the sensitivities obtained can be used in optimization. In particular, the project has demonstrated the optimization of a complex HSCT configuration with an aerodynamics analysis process that uses geometry and nonlinear aerodynamics analyses from the full multidisciplinary analysis, thus validating both the optimization formulation and the use of nonlinear CFD in an optimization process. These demonstrations and validations provide a sound basis for proceeding with implementation of the full multidisciplinary optimization.

The most important remaining activity to be performed is the formulation and implementation of the integrated *Sensitivity Analysis* process. The first attempts will involve perturbing a few design variables to get overall finite differences of the complete *Analysis* process. These differences can be used (1) to test the validity of the usual assumption that loads are constant for small design variable changes, (2) to perform a limited optimization of the perturbed design variables, and (3) to validate a later sensitivity derivative formulation that involves chain-ruling the individual derivatives from the component processes of the *Analysis* process. Once the *Sensitivity Analysis* process has been validated, complete optimizations can be run. The HPCCP CAS team plans to use the results from the HSCT4.0 multidisciplinary optimization to provide a baseline for future complex optimization projects.

References

[1]Walsh, J. L., Townsend, J. C., Salas, A. O., Samareh, J. A., Mukhopadhyay, V., and Barthelemy, J.-F., "Multidisciplinary High-Fidelity Analysis and Optimization of Aerospace Vehicles, Part 1: Formulation," AIAA Paper 2000-0418, Jan. 2000.

[2]Weston, R. P., Townsend, J. C., Eidson, T. M., and Gates, R. L., "A Distributed Computing Environment for Multidisciplinary Design," *Proceedings of the 5th AIAA/NASA/ISSMO Symposium on Multidisciplinary Analysis and Optimization*, Part 2, Panama City, FL, 1994, pp. 1091–1097.

[3]Krishnan, R., Sistla, R., and Dovi, A. R., "High-Speed Civil Transport Design Using FIDO," NASA CR-1999-209693, Oct. 1999.

[4]Balabanov, V. O., Kaufman, M., Giunta, A. A., Haftka, R. T., Grossman, B., Mason, W. H., and Watson, L. T., "Developing Customized Wing Weight Function by Structural Optimization on Parallel Computers," *Proceedings of the 37th AIAA/ASME/ ASCE/AHS/ASC Structures, Structural Dynamics and*

Materials Conference, Part 1, Salt Lake City, UT, 1996, pp. 113–125.

[5]Giunta, A. A., Balabanov, V. O., Haim, D., Grossman, B., Mason, W. H., Watson, L. T., and Haftka, R. T., "Wing Design for a High-Speed Civil Transport Using a Design of Experiments Methodology," *Proceedings of the 6th AIAA/NASA/ISSMO Symposium on Multidisciplinary Analysis and Optimization*, Part 1, Bellevue, WA, 1996, pp. 168–183.

[6]Giunta, A. A., and Sobieszczanski-Sobieski, J., "Progress Toward Using Sensitivity Derivatives in a High-Fidelity Aeroelastic Analysis of a Supersonic Transport," *Proceedings of the 7th AIAA/USAF/NASA/ISSMO Symposium on Multidisciplinary Analysis and Optimization*, Part 1, St. Louis, MO, 1998, pp. 441–453.

[7]Barthelemy, J.-F. M., Wrenn, G. A., Dovi, A. R., Coen, P. G., and Hall, L. E., "Supersonic Transport Wing Minimum Weight Design Integrating Aerodynamics and Structures," *Journal of Aircraft*, Vol. 31, No. 2, 1994, pp. 330–338.

[8]Hale, M., Craig, J. I., Mistree, F., and Schrage, D., "DREAMS and IMAGE: A Model and Computer Implementation for Concurrent, Life-Cycle Design of Complex Systems," *Concurrent Engineering: Research and Applications*, Vol. 4, No. 2, 1996, pp. 171–186.

[9]Guinta, A. A., "Sensitivity Analysis for Coupled Aero-Structural Systems," NASA / TM-1999-209367, Aug. 1999.

[10]Sobieski, I. P., Manning, V. M., and Kroo, I. M., "Response Surface Estimation and Refinement in Collaborative Optimization," *Proceedings of the 7th AIAA/USAF/NASA/ISSMO Symposium on Multidisciplinary Analysis and Optimization*, Part 1, St. Louis, MO, 1998, pp. 359–370.

[11]Weston, R. P., Green, L. L., Salas, A. O., Samareh, J. A., Townsend, J. C., Walsh, J. L., "Engineering Overview of a Multidisciplinary HSCT Design Framework Using Medium-Fidelity Analysis Codes," *1998 Computer Aerosciences Workshop*, NASA CP-20857, Jan. 1999, pp. 133–134.

[12]Sistla, R., Dovi, A. R., Su, P., and Shanmugasundaram, R., "Aircraft Design Problem Implementation Under the Common Object Request Broker Architecture," *40th AIAA/ASME/ASCE/AHS/ASC Structures, Structural Dynamics, and Materials Conference and Exhibit*, St. Louis, MO, 1999, pp. 1296–1305B.

[13]Sistla, R., Dovi, A. R., and Su, P., "A Distributed, Heterogeneous Computing Environment for Multidisciplinary Design & Analysis of Aerospace Vehicles," *5th National Symposium on Large-scale Analysis, Design and Intelligent Synthesis Environments*, Oct. 12–15, 1999, Williamsburg, VA.

[14]Vinoski, S., "CORBA: Integrating Diverse Applications Within Distributed Heterogeneous Environments," *IEEE Communications Magazine*, Vol. 14, No. 2, 1997, pp.46–55.

[15]Scotti, S. J., "Structural Design Using Equilibrium Programming Formulations," NASA TM-110175, June 1995.

[16]Woodward, F. A., "USSAERO Computer Program Development, Versions B and C," NASA CR-3228, Apr. 1980.

[17]Krist, S. L., Biedron, R. T., and Rumsey, C. L., "CFL3D User's Manual (Version 5.0)," NASA TM-208444, June 1998.

[18]Vanderplaats, G. N., *GENESIS User's Manual, Version 4.0*, VMA Engineering, Colorado Springs, CO, 1997.

[19]McCullers, A., "Aircraft Configuration Optimization Including Optimized Flight Profiles," *Proceedings of the Symposium on Recent Experiences in Multidisciplinary Analysis and Optimization*, edited by J. Sobieski, NASA CP-2327, Apr. 1984, pp. 396–412.

[20]Walsh, J. L., Young, K. C., Pritchard, J. I., Adelman, H. M., and Mantay, W. R., "Integrated Aerodynamic/Dynamic/Structural Optimization of Helicopter Rotor Blades Using Multilevel Decomposition," NASA TP-3465/ARL TR 518, Jan. 1995.

[21]Vanderplaats, G. N., "CONMIN—A Fortran Program for Constrained Function Minimization, User's Manual," NASA TM-X-62282, Aug. 1973.

[22]Samareh, J. A., "A Novel Shape Parameterization Approach," NASA / TM-1999-209116, May 1999.

[23]Biedron, R. T., Samareh, J. A., and Green, L. L., "Parallel Computation of Sensitivity Derivatives with Application to Aerodynamic Optimization of a Wing," *1998 Computer Aerosciences Workshop*, NASA CP-20857, Jan. 1999, pp. 219–224.

[24]Nielsen, E. J., and Anderson, W. K., "Aerodynamic Design Optimization on Unstructured Meshes Using

the Navier-Stokes Equations," *Proceedings of the 7th AIAA/USAF/NASA/ISSMO Symposium on Multidisciplinary Analysis and Optimization*, Part 2, St. Louis, MO, 1998, pp. 825–837.

[25]Mitchell, P. M., "Advanced Finite Element Weight Estimation Process on the High Speed Civil Transport," Society of Allied Weight Engineers, Biloxi, MS, SAWE Paper No. 2169, May 1993.

[26] Harris, R. V., Jr., "An Analysis and Correlation of Aircraft Wave Drag," NASA TMX–947, Mar. 1964.

[27]Bischof, C., Carle, A., Corliss, G., Griewank, A., and Hovland, P., "ADIFOR—Generating Derivative Codes from Fortran Programs, " *Scientific Programming*, No. 1, 1992, pp. 1–29.

[28]Bischof, C., Carle, A., Khademi, P., and Mauer, A., "The ADIFOR 2.0 System for the Automatic Differentiation of Fortran 77 Programs," 1994. CRPC-TR94491.

[29] Bischof, C., Carle, A., Hovland, P., Khademi, P., and Mauer, A., "ADIFOR 2.0 User's Guide (Revision D)," CRPC-TR95516-S, March 1995, Rev June 1998.

[30]Bischof, C., Roh, L., and Mauer, A., "ADIC—An Extensible Automatic Differentiation Tool for ANSI-C," Mathematics and Computer Science Division, Argonne National Laboratory, Technical Report ANL/MCS-P626-1196, Argonne, IL, 1996.

[31]Jones, W. T., and Samareh-Abolhassani, J., "A Grid-Generation System for Multidisciplinary Design Optimization," *Proceedings of the 12th AIAA Computational Fluid Dynamics Conference*, San Diego, CA, 1995, pp. 657–669.

Table 1 Typical timings

Process	Turnaround time	Computer type	Comments
Geometry	10 min	Silicon Graphics ORIGIN 2000[1] Silicon Graphics R10000[1]	Basic geometry section and ply analyses
Weights	5 min	Silicon Graphics R10000[1] Sun Ultra-2[2]	FEM theoretical weights as-built weights
Nonlinear Correction	3.3 hr	Silicon Graphics ORIGIN 2000[1] Silicon Graphics R10000[1]	CFL3D computations corrections application
Rigid Trim	2 min per load condition	3 Silicon Graphics[1] workstations Sun Ultra-2[2]	USSAERO computations trim iterations
Polars	1 hr	Silicon Graphics Octane	320 points, not parallelized
Performance	1 min	Sun Ultra-2[2]	
Ground Scrape	4 min	Sun Ultra-2[2]	
Displacements	3 min	Silicon Graphics R10000[1]	Cruise condition
Loads Convergence	4 hr	4 Silicon Graphics[1] workstations Silicon Graphics R10000[1] Sun Ultra-2[2]	USSAERO computations GENESIS® computations application (10 iterations)
Stress & Buckling	8 min	Silicon Graphics R10000[1]	
Analysis	5 hr (total)	All of the workstations above, with coarse-grain parallelization	With 10 iterations in *Loads Convergence*, but without *Nonlinear Corrections*

[1]Silicon Graphics, INDIGO, OCTANE, and ORIGIN 2000 are registered trademarks of Silicon Graphics, Inc.
[2]Sun is a registered trademark and Ultra-2 is a trademark of Sun Microsystems, Inc.

Table 2 Normalized sensitivities of empirical weight

	WING	FUSELAGE	STRUTOT	SYSTOT	OEW
XL	−0.479	0.801	−0.096	0.162	0.000
WF	−0.366	0.274	−0.149	0.251	0.000
DF	−0.315	0.325	−0.098	0.165	0.000
GTOW	0.627	0.132	0.544	0.051	0.255
AR	0.065	−0.024	−0.001	0.002	0.000
SW	0.887	0.156	0.510	0.115	0.257
SWEEP	−0.003	−0.003	−0.003	0.005	0.000

Table 3 Normalized performance sensitivities

	COMBND	RANGE	VAPP	FAROFF	FARLND	AMFOR	SSFOR
GTOW	−2.120	1.471	0.500	1.911	0.755	−0.618	−2.739
AR	−0.003	0.000	0.000	−0.003	0.017	0.000	0.029
SW	1.267	−0.402	−0.500	−1.086	−0.726	−0.002	−0.445
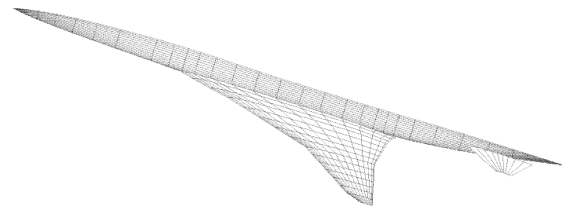
a) Linear aerodynamic grid

b) Finite element model

Fig. 1 High-Speed Civil Transport.
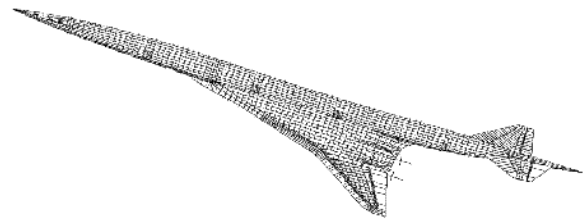
Fig. 2 Baseline HSCT4.0 model.
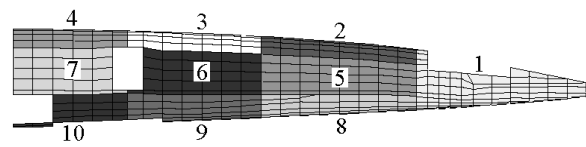
Forward fuselage
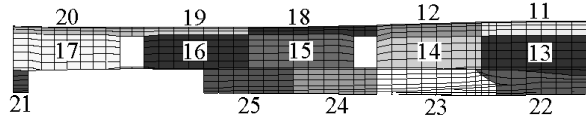
Middle fuselage
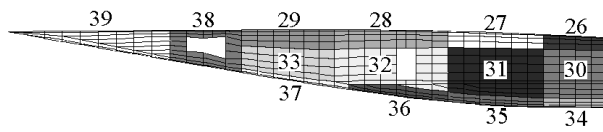
Aft fuselage
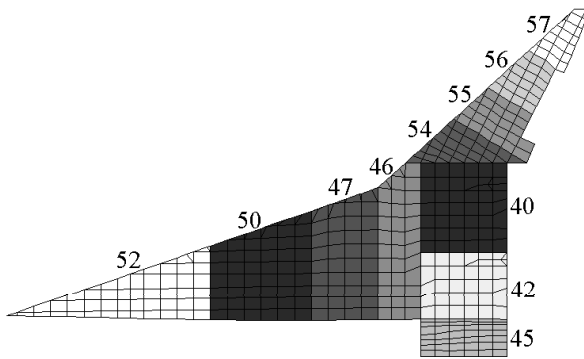
Upper wing
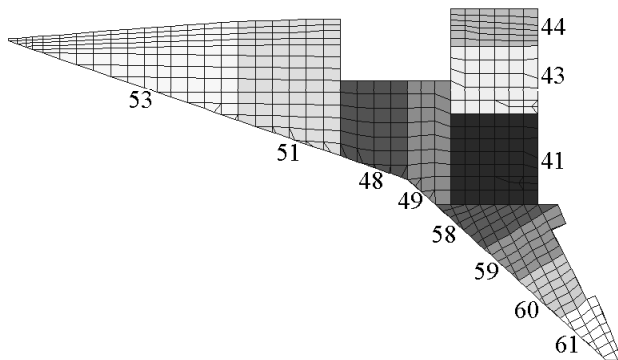
Lower wing

Fig. 3 Structural design zones.

0°
90°
Outboard wing
90° Fuselage
0°
90° Fuselage
90°
Inboard Wing
Inboard wing
0°

Face sheet
Core
Face sheet

$t_{0°}$
$t_{-45°}$
$t_{45°}$
$t_{90°}$
t_{Core}
$t_{90°}$
$t_{45°}$
$t_{-45°}$
$t_{0°}$

Fig. 4 Ply orientations and composite laminate stacking sequence.

C_3
SLE_3
SLE_2
Panel 3
C_2
Panel 2
B_3
Panel 1
B_2
L_n
C_r
L_t
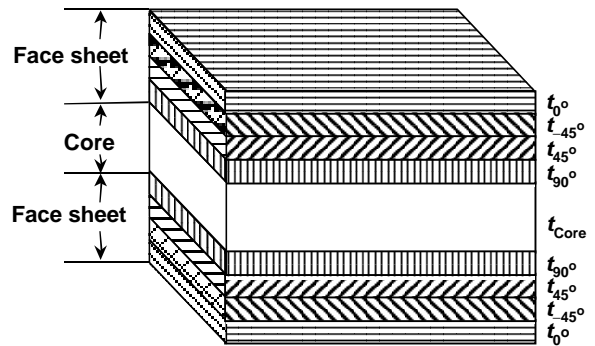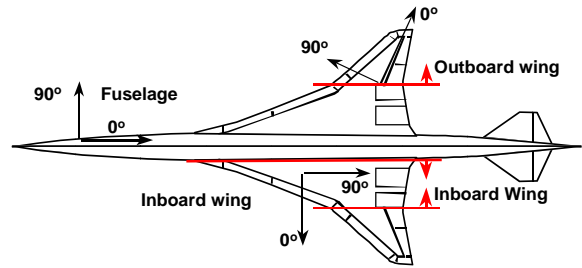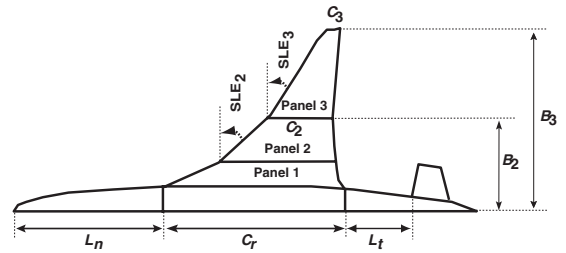
a) Planform design variables.

Δ_{shear}
Δ_{twist}
$\Delta_{thickness}$
Δ_{camber}

● ▲ ——— Modified wing
○ △ - - - - - Baseline wing

○ Airfoil camber
    definition points
○ Airfoil thickness
    definition points
△ Wing twist-angle vertex
    line definition points
△ Wing shear definition
    points
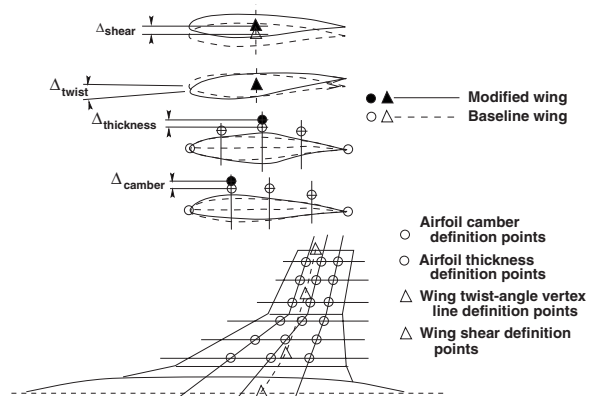
b) Wing camber, thickness, twist, and shear design variables.

Fig. 5 Shape design variables.
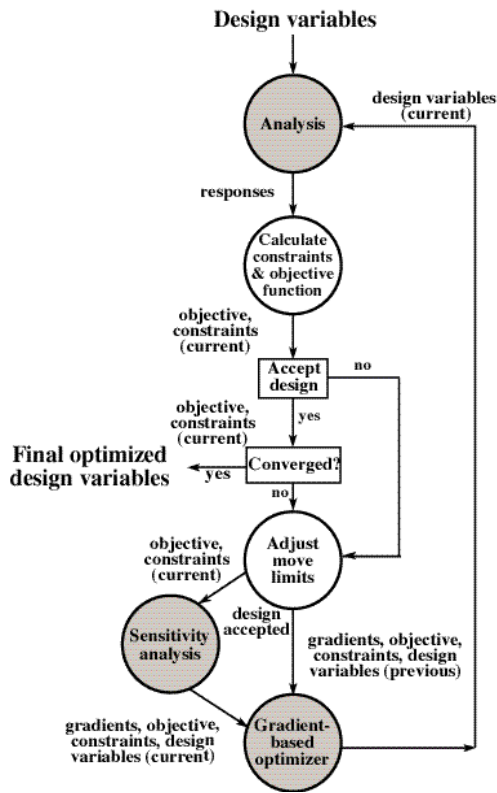
Fig. 6 *Optimization* **process.**
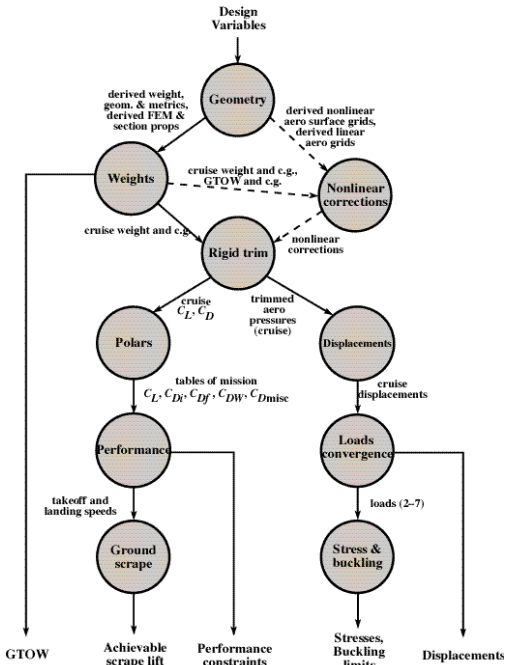
Fig. 7 *Analysis* **process.**
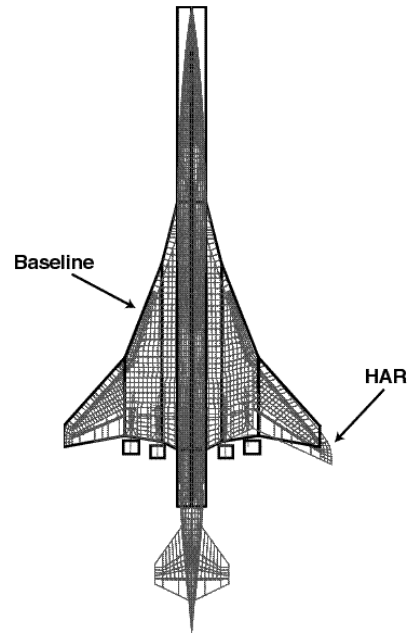
Fig. 8 HSCT4.0 FEM geometry parameterization.
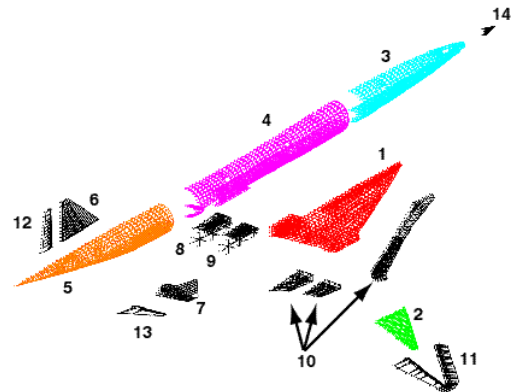
Fig. 9 Weight calculation regions.
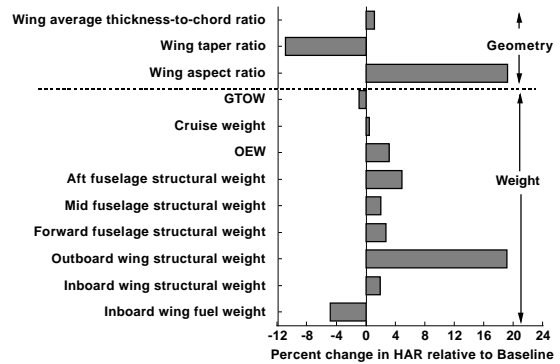
Fig. 10 Normalized weight and geometry changes.

15
American Institute of Aeronautics and Astronautics

a) 2.5g load condition

a) Baseline configuration
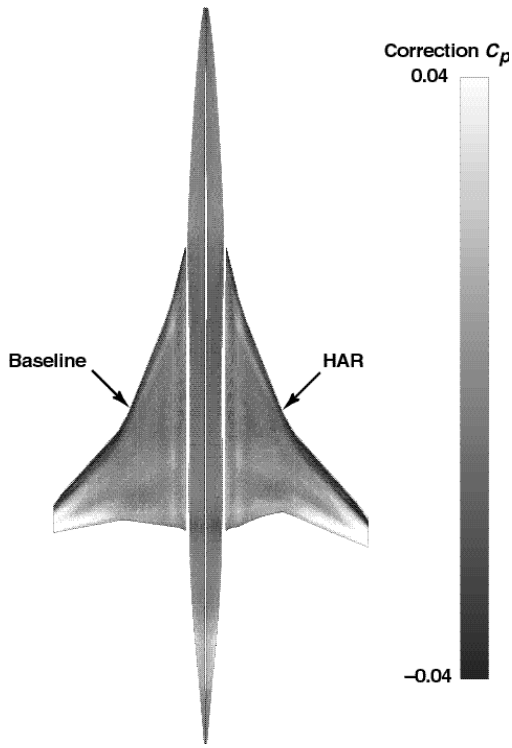
b) HAR configuration
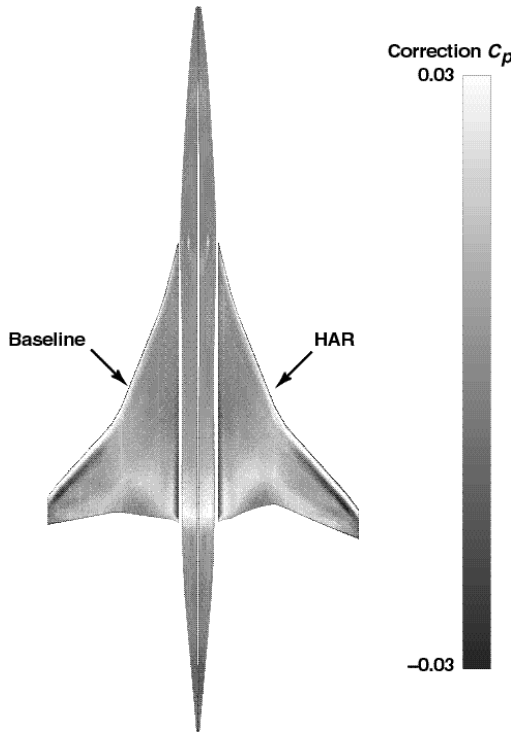
Fig. 12 Drag polars.

b) –1g load condition

Fig. 11 Nonlinear corrections in terms of C_p.
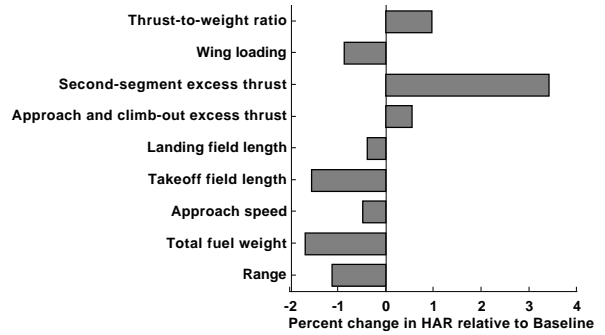
Fig. 13 Normalized performance comparison.
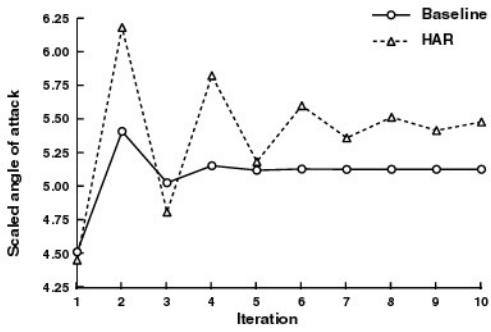
a) Scaled angle of attack, 2.5g load condition

a) Baseline configuration, 2.5g load condition
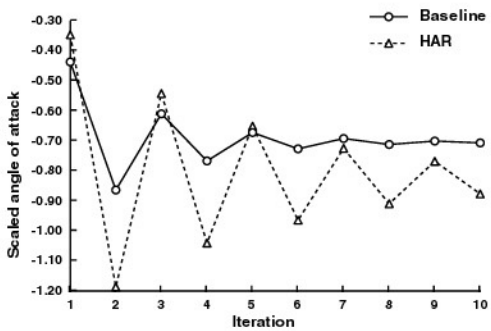
b) Scaled angle of attack, −1g load condition

b) Baseline configuration, −1g load condition
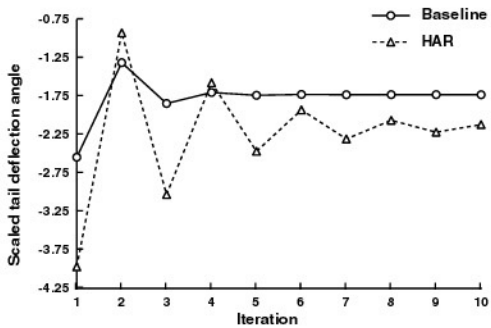
c) Scaled tail deflection angle, 2.5g load condition

c) HAR configuration, 2.5g load condition
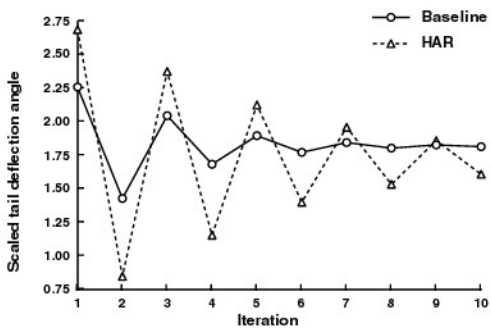
d) Scaled tail deflection angle, −1g load condition

Fig. 14 Loads convergence histories.
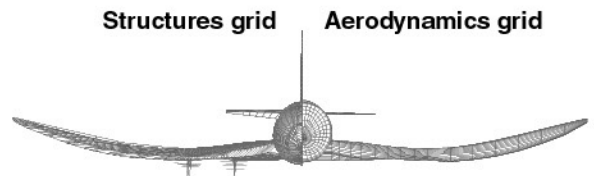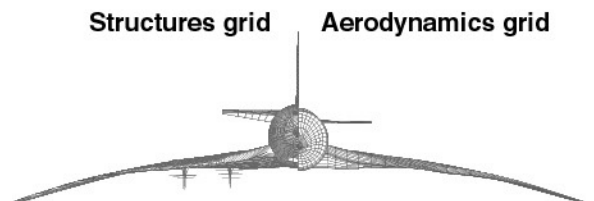
d) HAR configuration, −1g load condition

Fig. 15 Final converged shapes.

American Institute of Aeronautics and Astronautics
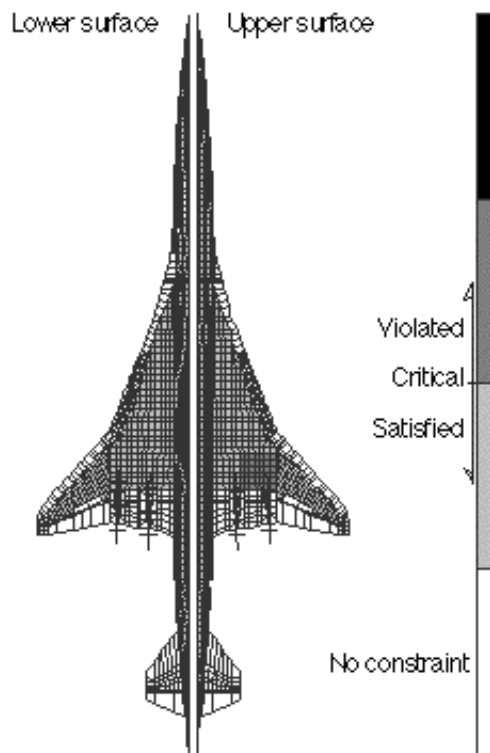
(a) 2.5g load condition
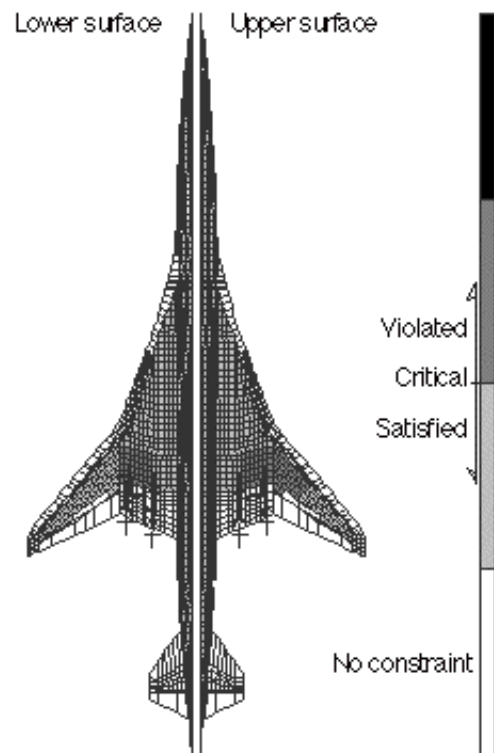
(a) 2.5g load condition
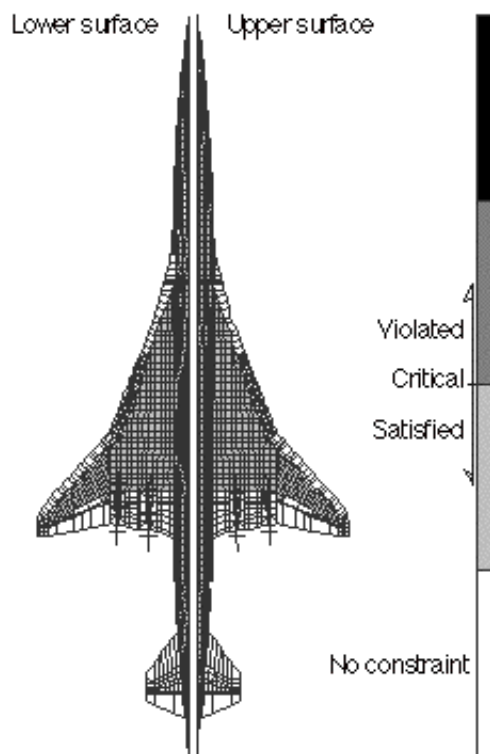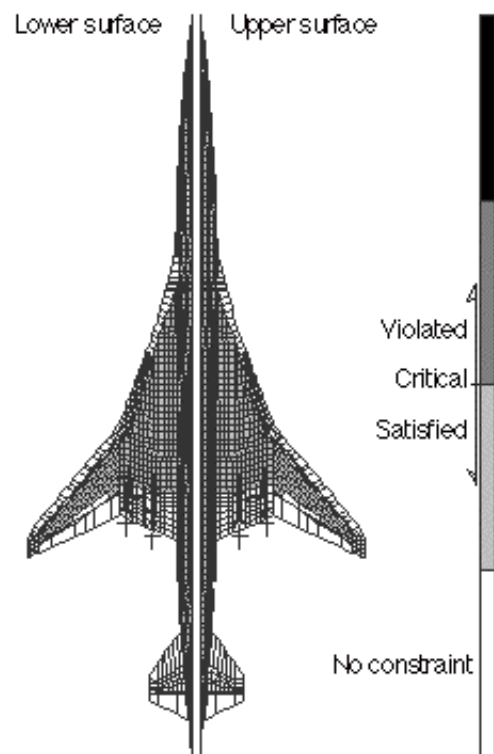
(b) −1g load condition

(b) −1g load condition

Fig. 16 Stress failure index for Baseline configuration.

Fig. 17 Stress failure index for HAR configuration.
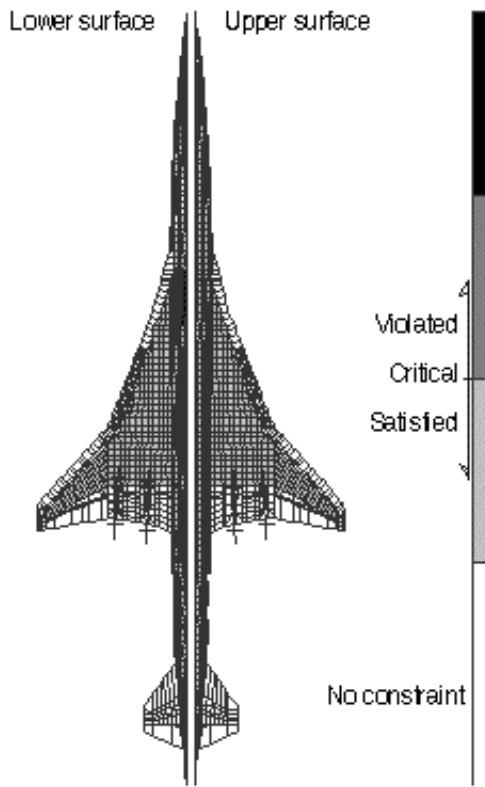
(a) 2.5g load condition
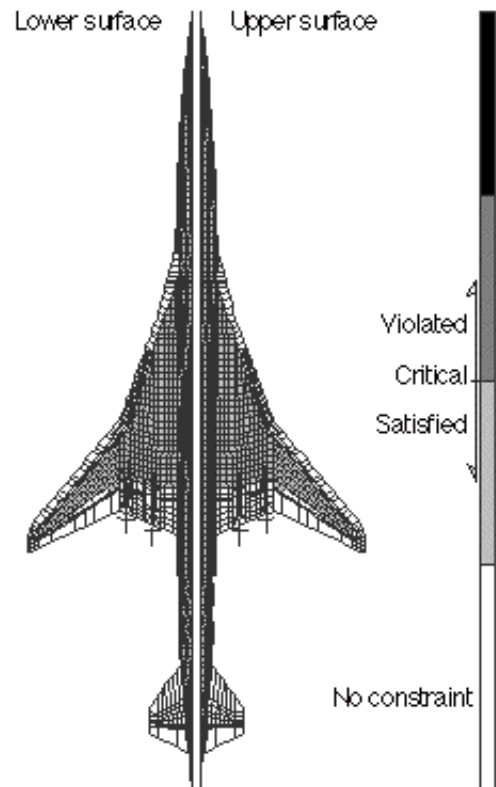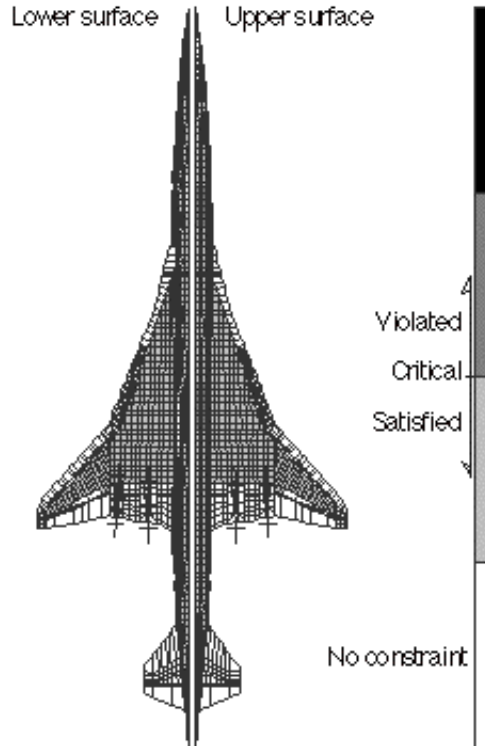
(a) 2.5g load condition
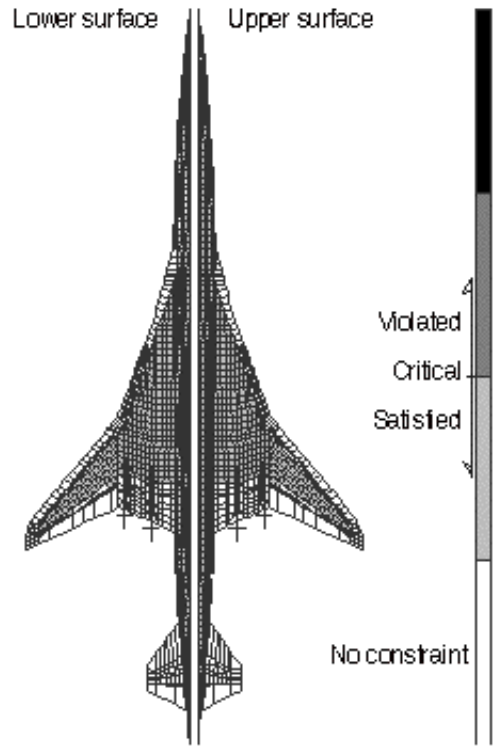
(b) −1g load condition

Fig. 18 Buckling load factor for Baseline configuration.

(b) −1g load condition

Fig. 19 Buckling load factor for HAR configuration.
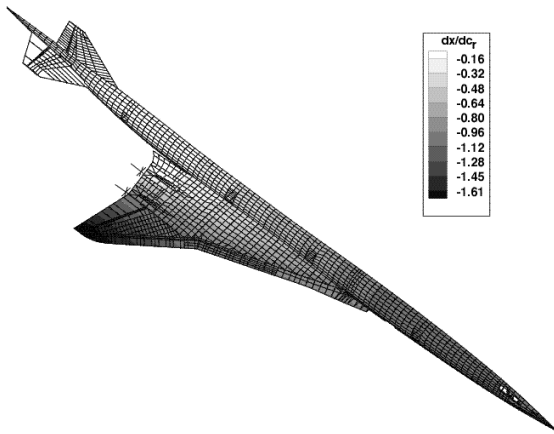
Fig. 20 FEM shape sensitivity.

Fig. 21 Nonlinear CFD volume grid sensitivity.

Fig. 22 *Analysis* **process for nonlinear aerodynamic optimization.**
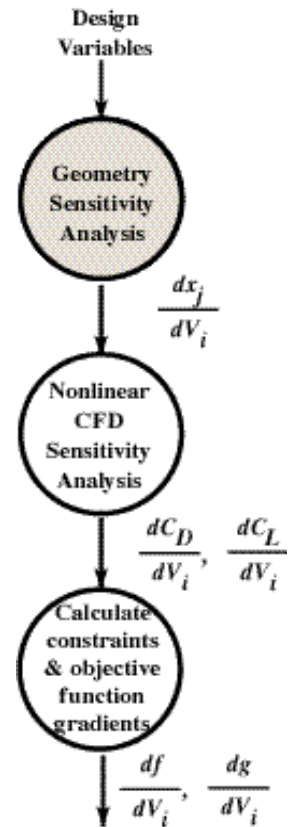
Fig. 23 *Sensitivity Analysis* **process for nonlinear aerodynamic optimization.**

Fig. 25 Aerodynamic shape optimization history.
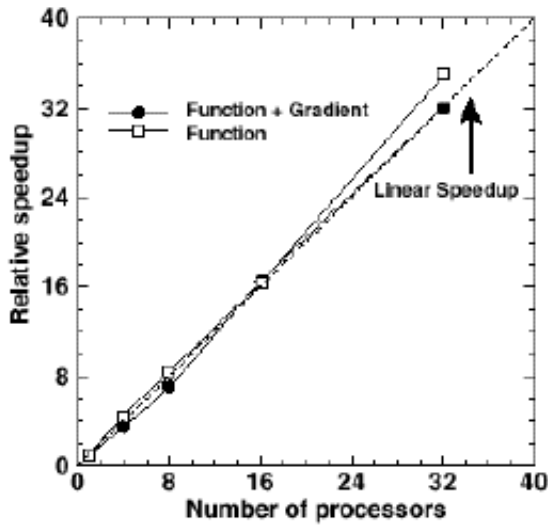
Fig. 24 Speedup relative to a single processor for function and function-plus-gradient evaluation on a 195MHz Silicon Graphics Origin 2000.
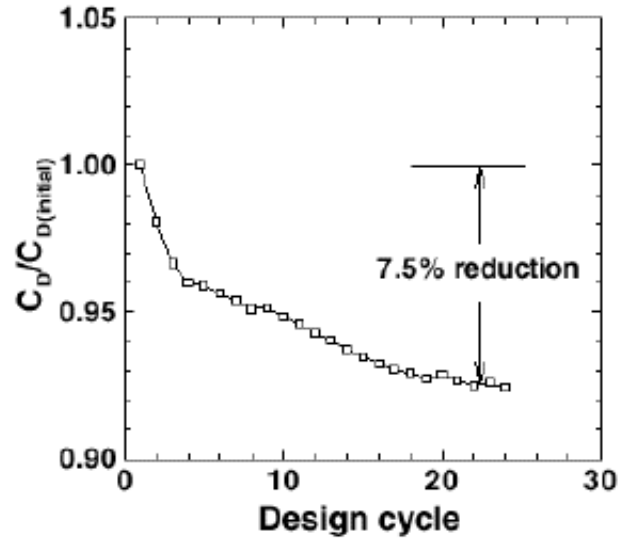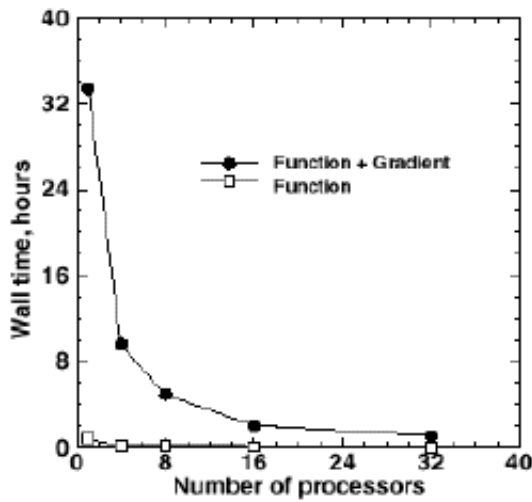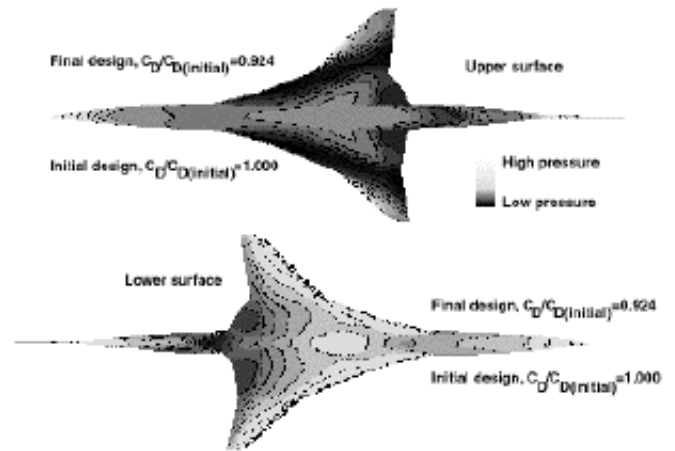

Fig. 26 Baseline and final surface pressures from aerodynamic shape optimization.